Thorium distributions in high- and low-dust regions and the significance for iron supply

Citation: Hayes, Christopher T., Jeffrey Rosen, David McGee, and Edward A. Boyle. "Thorium Distributions in High- and Low-Dust Regions and the Significance for Iron Supply." Global Biogeochemical Cycles 31 (January 2017): 328-347 © 2017 American Geophysical Union

As Published: https://doi.org/10.1002/2016GB005511

Publisher: American Geophysical Union (AGU)

Persistent URL: http://hdl.handle.net/1721.1/120502

Version: Original manuscript: author's manuscript prior to formal peer review

Thorium distributions in high and low dust regions and the significance for iron supply

Christopher T. Hayes, David McGee, Jeffrey Rosen, Edward A. Boyle

The long-lived Th isotopes (^{232}Th and ^{230}Th) and ^{234}U/^{238}U ratios were analyzed on a transect cruise between Barbados and Bermuda, intersecting the Saharan dust plume, in an effort to refine their use for estimating mineral dust deposition and Fe delivery. Near Barbados, waters affected by the Amazon outflow contain elevated ^{232}Th. This signals one region where the thorium-dust method is inaccurate because of a confounding continental input, but the potential for ^{232}Th to constrain Amazonian Fe delivery is also discussed. The colloidal content of dissolved Th south of Bermuda was found to be quite small (2-6%), similar to that found north of Hawaii, despite the order of magnitude higher dust deposition in the Atlantic. It appears that Fe concentrations in the remote ocean are highly buffered by a combination of biological uptake, scavenging and ligand availability, whereas ^{232}Th has a larger dynamic range between high and low dust regions, further demonstrating its ability to trace lithogenic supplies. Outside the Amazon influence, dissolved ^{232}Th fluxes in the mixed layer and integrated from surface to 500 m depth are used with concurrently Bermudan aerosol deposition to estimate that fractional Th solubility, while still highly unconstrained, is close to 20%.

Formatted: Highlight

1. Introduction

Marine chemists have conceived of the surface ocean as a "large, uncalibrated dust collector that integrates the high frequency temporal aspect of atmospheric dust input" [*Measures and Brown*, 1996]. Quantifying atmospheric dust input to the ocean is a key motivation in studying the biogeochemical cycles of bioactive or pollutive elements which have a significant source in dust, such as Fe, N, P, Pb, etc. Using trace metals that partially solubilize from dust, one can calibrate the surface ocean dust collector by assuming a steady-state balance for the inventory of the dissolved metal between supply, by dust dissolution, and removal, by scavenging onto sinking particles. This approach was developed for the case of aluminum as "Measurement of Al for Dust Calculation in Oceanic Waters" or the MADCOW model [*Measures and Brown*, 1996; *Measures and Vink*, 2000]. Analogous approaches have been proposed for titanium [*Dammshäuser et al.*, 2011], gallium [*Shiller and Bairamadgi*, 2006], and thorium [*Hirose and Sugimura*, 1987; *Huh et al.*, 1994; *Hsieh et al.*, 2011; *Hayes et al.*, 2013].

The use of thorium, having both primordial (^{232}Th) and radiogenic (e.g., ^{230}Th) isotopes, offers some advantages over the other lithogenic metals in that its residence time with respect to scavenging can be directly measured from radioactive disequilibria, e.g., between ^{234}U and ^{230}Th. Uncertainties in the use of Th isotopes for dust estimates and for dissolved Fe supply have developed [*Hayes et al.*, 2015c; *Anderson et al.*, 2016], however, including the correct integration depth for Th inventories, sources of Th other than dust, Th size speciation and isotope equilibrium and Th solubility. These issues provide the focus of this study. Here, we investigated ^{232}Th, ^{230}Th and ^{238}U/^{234}U distributions in the relatively high aerosol dust deposition environment of the northwest subtropical Atlantic.

In Results (Sec. 3), we introduce the new hydrographic and chemical measurements made across a transect between Barbados and Bermuda (Fig. 1). Further, we show how the data indicate that care must be taken in how ^{232}Th and ^{230}Th are integrated when the goal is to estimate fluxes of lithogenic materials, such as dust deposition. In particular, the data suggest that integration below the mixed, to sub-euphotic zone depths may be necessary. Also in Results, despite some published findings suggestive of the contrary, we found no evidence for non-conservative behavior of U concentrations or isotope composition in the studied region.

In the Discussion (Sec. 4), we first illustrate how sources other than aerosol dust can bias dust estimates using data from stations impacted by the Amazon outflow. Secondly, we find that only a small percentage of dissolved Th exists in the colloidal size range even under conditions of high dust deposition where dissolved Fe is substantially colloidal. Finally, we find that comparisons between integrated dissolved ^{232}Th fluxes with aerosol deposition estimates indicate that Th solubility is largely unconstrained and presents the greatest need for future research in dissolved metal proxies for mineral dust deposition.

2. Material and Methods

2.1 Sample collection

The samples used in this study were collected on a UNOLS Chief Scientist Training Workshop cruise (http://csw2014_1.unols.org/) on May 31-June 8, 2014 that ran as a transect from Barbados to Bermuda aboard the R/V *Atlantic Explorer* (cruise number AE1410). Eight stations were occupied (Fig 1) for water sampling, and aerosol samples were collected during transits between stations. Water samples were collected with the ship's Niskin bottle rosette, using GEOTRACES protocols for radionuclides. For Th isotopes, 5 L each of unfiltered and filtered (0.45/0.8 μm Acropak cartridge) seawater was sampled into acid-cleaned cubitainers,

using Teflon-coated Tygon tubing. Water samples were acidified aboard ship to pH 1.8 using ultra-clean 6 M hydrochloric acid. Dissolved U concentrations and isotopes were analyzed on 3-5 mL sub-samples of the filtered water used for Th analysis.

At station 6, prior to sample acidification, we performed 10 kDa membrane cross flow filtration (CFF) of the 0.45 µm filtered water to determine the colloidal content of the dissolved ^{232}Th. The same protocols were followed as reported by Hayes et al. [2015], except that volume sizes were limited to processing 2.5 L of pre-filtered seawater for CFF, using 500 mL to precondition the system and collecting 0.8-1.0 L for permeate and retentate fractions. Recovery of Th was 95-100%.

Aerosol samples were collected with a Tisch Environmental (TE-6070) PM10 air sampler. New 8"x10" Whatman41 regenerated cellulose filters were loaded into a stainless steel mesh filter holder with anodized Al housing. To avoid contamination from the ship's exhaust the air sampler pump was only powered when the wind was greater than 1 m/s and within 180 degrees of the bow, using a power switch in conjunction with an anemometer mounted above the sampler. The time pumped and average flow rate, used for sample volume, was recorded using a pen chart recorder in addition to a digital data logger. Flow rates ranged from 44-54 cubic feet per minute, and sample volumes ranged from 307 to 1584 cubic meters. Loading of aerosol material on the filters was visually uniform.

2.2 Analytical procedures

Th isotopes were analyzed by isotope-dilution mass spectrometry using a Nu Plasma II at MIT following acid digestion and chromatographic purification described by Hayes et al. [2015]. The average and standard deviation of procedural blanks in these samples sets (n = 6) were 0.014 ± 0.007 pmol ^{232}Th and 0.13 ± 0.20 µBq ^{230}Th, comprising less than 2% and less than 3% of the

smallest seawater sample sizes analyzed for ^{232}Th and ^{230}Th, respectively. Reproducibility and accuracy was monitored by analysis of a seawater standard (SWS2010-1, [*Anderson et al.*, 2012]), and percent differences between measured values and the consensus values for both Th isotopes ranges from 0-4%.

U analysis was also performed using isotope dilution, using ^{236}U, on the Nu Plasma II. A method similar to that reported by Reuer et al. [2003] for Pb isotopes, was used involving $Mg(OH)_2$ co-precipitation and purification by anion-exchange resin (AG1-X8) prior to mass spectrometry. We are not aware of a seawater U standard. Reproducibility was monitored by sample replicate analysis (Jeff, insert values here) and a commercially available ICP-MS uranium standard (detail needed here?).

For Th isotope analysis of the aerosol samples, sub-sections of the filter were cut with ceramic scissors and the area fraction of the whole sample was used to calculate sample size. Filter and aerosols were dissolved using a combination of nitric acid and hydrofluoric acid in sealed PFA-vessels heated to 150°C, similar to methods described by Morton et al. [2013]. Once dissolved, aerosol Th samples were purified and analyzed as with seawater samples. Blank filters (n = 3) were cut to the same size as samples, dissolved and analyzed to determine the full procedural blank. These averaged 0.86 ± 0.01 pmol ^{232}Th. This represented < 2% of the ^{232}Th in the samples from the beginning of the cruise until Station 4, which had the highest aerosol loadings. Between stations 4 and the end of the cruise, samples had lower aerosol loadings and here the filter blank represented 5-30% of the samples analyzed.

All data reported here are available in the Supplemental Material. The Th isotope data will also be included in the GEOTRACES Intermediate Data Product 2017, as GEOTRACES-compliant data.

Formatted: Highlight

Formatted: Highlight

Formatted: Highlight

Commented [EB1]: It is news to me that U concentrates with Mg(OH)2. It seems that almost everything except NaCl does!

Commented [EB2]: Weyer(2008)GCA72_345 analyzed surface seawater samples from Bermuda and Hawaii, this might serve as a basis for comparison.

Formatted: Highlight

Commented [EB3]: It would be worth noting whether this was depleted uranium standard. Doesn't matter much from this concentration perspective, but we still should say this.

2.3 Thorium excess and flux calculations

A unique feature of Th is that it has an isotope composition that can be used to distinguish terrestrial versus oceanic sources. Th-232 is a primordial component of continental rocks and the ^{230}Th present in continental material is typically close to secular equilibrium with the ^{238}U found in those rocks. Under this assumption, the average upper continental crust has a ^{230}Th/^{232}Th atom ratio of 236,000 [*Rudnick and Gao*, 2014]. This isotope ratio for continental material in the ocean is consistent with that measured in sediment traps in the Mediterranean Sea of 250,000 ± 6000 [*Roy-Barman et al.*, 2009]. Th produced from uranium dissolved in seawater, on the other hand, is mono-isotopic as ^{230}Th (excluding the other radiogenic Th isotopes which constitute a near-negligible mass fraction because of their short half-lives). Therefore, one can isolate the fraction of seawater ^{230}Th produced by dissolved uranium decay (^{230}Th xs) by subtracting the quotient of measured seawater ^{232}Th and the lithogenic isotope ratio (Eq. 1). This correction can be applied to both dissolved samples and total dissolvable (dissolved plus particulate) samples.

$$^{230}Th\ xs = {}^{230}Th_{meas} - {}^{232}Th_{meas} \div \left(\frac{^{232}Th}{^{230}Th}\right)_{litho} \qquad \text{Eq. 1}$$

As in previous reports [*Hayes et al.*, 2013, 2015c], we consider dissolved ^{232}Th fluxes in an integrated sense. Conceptually, aerosol mineral dust is deposited at the sea surface and will then undergo a complex journey involving being mixed throughout the mixed layer, possibly undergoing rapid particle packaging and sinking concurrent with the downward export of organic carbon and partial dissolution throughout these processes. Largely because we have no prior reason to expect that dust particle dissolution processes should be confined to the mixed layer, we extend the integration of Th inventories below the mixed layer in contrast to other approaches [*Hsieh et al.*, 2011; *Deng et al.*, 2014]. Five hundred meters was used as a benchmark in previous

work based on the structure of dissolved ^{232}Th depth profiles in the North Pacific, but conceptually any integration depth may be used here.

The integration depth deemed appropriate for ^{232}Th cycling is then used as the depth to which a dissolved Th residence time based on the integrated radioactive disequilibrium between the homogeneous, soluble parent ^{234}U and the scavenged daughter dissolved ^{230}Th. Because the half-life of ^{230}Th is much longer than its residence time in the water column, the residence time can be defined simply from the ratio of the inventory of dissolved ^{230}Th to the integrated production of ^{230}Th by ^{234}U decay (P_{230}). A dissolved Th flux is then converted into a mineral dust flux (Eq. 2), or a dissolved metal flux from dust, defined for Fe in Eq. 3, using the fractional Th solubility for dust (S_{Th}) and concentration in dust (Th_{dust}), or the relative fractional solubility of the metal and thorium, respectively. The second term on the right side of these equations is the inverse of the residence time. P_{230} is a function of salinity and is 0.43 μBq/dm^3/yr at salinity 35.

$$F(dust) = \int_0^z d^{232}Th\, dz \times \frac{\int_0^z P_{230}\, dz}{\int_0^z d^{230}Th\, dz} \times \frac{1}{S_{Th} \times Th_{dust}} \qquad \text{Eq. 2}$$

$$F(dFe) = \int_0^z d^{232}Th\, dz \times \frac{\int_0^z P_{230}\, dz}{\int_0^z d^{230}Th\, dz} \times \frac{S_{Fe}}{S_{Th}} \qquad \text{Eq. 3}$$

3. Results

3.1 Hydrography

A significant feature of the beginning of this cruise track was the lower salinity waters derived from the Amazon and Orinoco River outflows (Fig. 1). The influence of river runoff in this area is seasonal with the strongest outflows occurring between May and November [*Steven and Brooks*, 1972; *Hellweger and Gordon*, 2002]. Moore et al. [1986] estimated that 20-34% of the surface water east of the Lesser Antilles in June is derived from the Amazon estuary. Our transect exited the Amazon-influenced waters at about 15°N (Figs. 1, 2A). North of here, we

Commented [EB4]: As I mentioned at the Royal Society meeting, because seawater Th has a high 230Th/232Th ratio compared to crustal material, there might be some degree of isotope equilibration going on when continental dust hits the ocean. I wonder if that is a partial explanation for the release of Th232 below the mixed layer – the deeper water has a higher 230Th/232Th ratio.
To think about this, we need to have the 230 and 232 in the same units (if the ^{230}Th concentration is much lower, it couldn't exchange enough to matter) – could you make a data table that does this? Oh, now I see the same units on Figure 5, and it appears that seawater 230Th is indeed high enough to do some isotope exchange.

crossed the tropical-subtropical front expressed by boundary between the North Equatorial Current and the subtropical gyre. This boundary is climatologically around 20°N [*Eden and Willebrand*, 2001] at this longitude. The edge of the subtropical gyre is visible in the salinity field seen in Fig. 1 just south of the front of salinities higher than 37.

Our sampling was restricted to the surface water (10 m depth) for stations 1, 3, 5, and 7, and to the upper 500 m at stations 2, 6 and 8. The vertical structure of water masses at stations 6 and 8 are similar, and station 8 is coincident with the Bermuda Atlantic Time-series Station (BATS) [*Lomas et al.*, 2013]. Typical of summer, mixed layers are shallow at these stations (15 m), which overlay a seasonal thermocline extending to 100-150 m depth. Below the seasonal thermocline is a roughly 200 m slab of 18°C water, or subtropical mode water (Fig. 2). The thickness of the 18°C water contracts going south in the section and is nearly gone by station 3. At stations 1-3, a clear subsurface salinity maximum is visible, indicative of subtropical underwater (salinity 37, ~20° C) which has been subducted and advected from the subtropical gyre [*Blanke et al.*, 2002]. Below the subtropical underwater at stations 1-3, we found thermocline waters, consistent with ventilation from North Atlantic Central Water [*Poole and Tomczak*, 1999]. Only at stations 1 and 2 did we find low surface (upper 50 m) salinity anomalies indicating a contribution from the Amazon outflow.

3.2 Surface transects

We traversed the Saharan dust plume which was present over the Lesser Antilles in late Spring 2014 and ended with a very sharp front around 20°N, according to Terra MODIS Aerosol Optical Depth (see Supplemental Material). This was abundantly clear in the aerosol ^{232}Th data (Fig. 3A) which showed a maximum of 3.8 pmol per cubic meter of air in the sample collected between 15.6 and 22.2°N and dropped to <0.06 pmol/m^3 further north. Aerosol filters were

178 visibly red-brown, indicative of iron oxides from Saharan dust, until 22.2°N, north of which
179 filters did not display significant coloration.

180 Dissolved ^{232}Th in surface waters (10 m depth) shows a less dramatic latitudinal
181 variability, about a factor of 2 higher in the south than in the north and its peak at St. 2, in waters
182 affected by the Amazon outflow (Fig. 1). The concurrence of lowered salinity and increased
183 seawater Th is suggestive that the Amazon outflow could be a substantial source of Th to the
184 adjacent ocean. Total dissolvable ^{232}Th, which includes particulates, likely represents some of
185 the higher frequency seasonal input of dust with very high concentrations at St. 4 (22.2°N).
186 Excluding that station, particulate ^{232}Th represented 19 ± 8 % (average and 1 standard deviation)
187 of the total dissolvable ^{232}Th, which is typical of that reported from other oceanic areas [*Roy-*
188 *Barman et al.*, 1996; *Hayes et al.*, 2015a].

189 The data from surface ^{230}Th transect clearly demonstrate the power of ^{230}Th xs as an
190 indicator of scavenging intensity and the adequacy of the lithogenic correction based on ^{232}Th. In
191 Fig. 3B, we plot both measured and the dissolved xs concentrations. In the southern part of the
192 transect that has more ^{232}Th, the corrections are noticeably larger and constitute a substantial
193 fraction of the measured ^{230}Th (up to 60% at Station 2). We have an independent metric for
194 scavenging intensity which is the beam attenuation coefficient, measured by transmissometer.
195 The beam attenuation coefficient is linearly related to particle concentration [*Gardner et al.*,
196 1985; *Bishop*, 1986] and is inversely related to dissolved ^{230}Th xs across the Atlantic [*Hayes et*
197 *al.*, 2015a]. As one validation for the accuracy of the lithogenic correction, the least-squares
198 coefficient of determination (R^2) between dissolved ^{230}Th and beam attenuation coefficient
199 increases from 0.41, using measured data, to 0.91, using dissolved ^{230}Th xs. The range in
200 residence times with respect to scavenging across this transect is 2.8 years at the most

oligotrophic station 6 to 1.2 years at St. 2 which had the highest surface water particle abundance.

As another validation of the lithogenic correction, as well as a good demonstration of the terrestrial-oceanic Th isotope mixing relationship, in Fig. 4, we show the Th isotope ratio as a function of latitude. The aerosol samples all fall within 200,000 and 260,000, centering over the UCC average of 236,000. This is a tighter ratio distribution than that measured on Saharan dust particles collected over a year in Monaco rain ($^{232}Th/^{230}Th$ = 170,000-250,000) [*Pham et al.*, 2005]. Therefore, we may have sampled aerosol dust from a relatively homogeneous, or geographically limited, source in ~~the Sahara~~North Africa.

Commented [EB5]: Sahel could also be a source

The seawater $^{232}Th/^{230}Th$ ratios rise from about 50,000 near Bermuda to roughly 150,000 in the Amazon outflow waters. The unfiltered samples rise to close to the crustal ratio at stations 2 and 4, indicating recent additions of lithogenic material. We note that while this ratio is sensitive to the mixture of lithogenic versus "hydrogenic" Th, we do not have enough information on the isotopic composition of riverine Th from the Amazon to distinguish this lithogenic source from Aeolian Th.

3.3 Depth profiles

In depth profiles to 500 m from stations 2, 6, and 8 (BATS), several of the trends seen in latitudinal variation can be seen in more detail (Fig. 5). We focus here on dissolved ^{232}Th, as total dissolvable ^{232}Th shows similar distribution to the dissolved data (particulate Th being 19 ± 10% of dissolved on average in the profile data) and dissolved ^{230}Th xs, as this parameter isolates the spatial variability in scavenging intensity. Total dissolvable ^{230}Th measurements indicated an average and standard deviation of 20 ± 14 % of the total ^{230}Th was particulate. In some cases, the calculated particulate ^{230}Th was below detection, or not statistically distinguishable from zero.

Using the difference between filtered and unfiltered samples, at least with 5 L samples for shallow water (upper 500 m) in this region, may not be the optimal method to determine particulate ^{230}Th, whereas particulate ^{232}Th appeared to be well-resolved.

The fresher water in the upper 35 m of the water column at St. 2, affected by the Amazon outflow, is clearly seen with elevated ^{232}Th. As in previous work [*Hayes et al.*, 2015c], there is a local minimum in dissolved ^{232}Th concentration at the depth of the deep chlorophyll maximum (DCM), as indicated by fluorescence. The depth of the DCM, and the local minimum in ^{232}Th, ranges across this transect from the shallowest at 35-50 m at St. 2, to its deepest (150 m) at the most oligotrophic St. 6, to shallower again (100 m) at St. 8. The biological production and packaging of particles in the euphotic zone likely plays a strong role in scavenging ^{232}Th.

The dissolved ^{230}Th xs profiles also display variation related the fluorescence profile similar to what was observed in time-series profiles from Station ALOHA [*Hayes et al.*, 2015c]. While the model of reversible scavenging predicts a simple linear increase with depth of ^{230}Th concentrations, in our observations, dissolved ^{230}Th xs concentrations are nearly invariant between the surface and the depth of the deep chlorophyll maximum (DCM) (Fig. 4 C-D). Only below the DCM does the linear increase in concentration with depth begin. This is crucially important for how dissolved Th isotopes are used in estimating aerosol dust deposition. Firstly, ^{230}Th appears to be "mixed", i.e. homogeneous in concentration, above the DCM (35, 150 and 100 m respectively for stations 2, 6, and 8), rather than only in the physical mixed layer. The physical mixed layers (22, 15 and 15 m, respectively for stations 2, 6, and 8), based on a potential density change greater than 0.125 kg/m^3, are significantly shallower than the DCM's. The consequence of this phenomenon is that the dissolved Th residence time derived from this data (Fig. 4E) will be the same using any integration depth between the surface and the DCM.

The inventory of dissolved ^{232}Th increases significantly between the base of the mixed layer and the DCM, while as mentioned the residence time remains constant. Therefore the derived dissolved ^{232}Th flux will increase with integration depth (Fig. 5F), most likely simply because of the effect of the Th residence time.

Put another way, the reversible scavenging model does not appear to apply to oceanic waters above the DCM (or perhaps bounded by the euphotic zone) and this is potentially problematic for the combined use of long-lived thorium isotopes for dissolved flux estimates. We hypothesize that there is a type of irreversible scavenging for both ^{230}Th and ^{232}Th that occurs in the euphotic zone that causes a downward export of Th out of euphotic with possible regeneration of dissolved Th below the euphotic zone, as is observed for ^{234}Th [*Maiti et al.*, 2010]. Higher depth-resolution sampling of dissolved and particulate ^{232}Th/^{230}Th in the upper 250-500 m of the water will be required to test this hypothesis. As we found, particulate ^{230}Th was not readily resolvable using the unfiltered minus filtered approach used here, and thus in-situ pumping is more likely to be successfully resolve the scavenging dynamics in the euphotic zone.

At this point, in order to use the integrated ^{232}Th/^{230}Th inventories as proxies for total lithogenic supplies, such as aerosol dust deposition, we suggest the integration should be done at least to sub-euphotic zones depths (>150 m, in most cases). This export depth effect is also likely to influence the fluxes used to estimate dissolved trace element supply [*Hayes et al.*, 2015c]. Nonetheless, with this integration-depth uncertainty in mind, we use these fluxes, which are quantifiable based on robust radioactive principles, as our current best estimates in the Discussion section to investigate Amazon Fe supplies and Th solubility.

3.4 Uranium isotope distribution

We investigated ^{238}U concentrations and $^{234}U/^{238}U$ ratios in the filtered seawater in this dataset for three reasons. Firstly, ^{234}U is a necessary parameter estimating Th residences times and fluxes but is often simply assumed based on its conservative behavior in the ocean using a uranium-salinity relationship covering only a few locations in the ocean [*Owens et al.*, 2011]. Secondly, Owens et al. [2011] reported several samples from the BATS site (Fig. 1), in particular, that had considerably depleted U concentrations compared to that expected from salinity. Thirdly, there is evidence for non-conservative behavior (U removal) and a U isotope source distinct from seawater in the Amazon estuarine zone [*Swarzenski et al.*, 2004]. The Amazon outflow partly influences surface waters, at least in terms of salinity, at stations 1 and 2 of this transect (Fig. 1).

Commented [EB6]: I think that later Stephanie more or less retracted the contention of non-conservative U because they never saw it again. Maybe in her thesis? Or ask her if there's a reference?

We found, however, no evidence for non-conservative U behavior or significant isotope variation in this sample set. Our ^{238}U estimates agreed within 1 sigma uncertainty with that predicted by CTD salinity and the U-salinity relationship from Owens et al. [2011] for all but three of the dissolved samples (and these agreed within 2 sigma uncertainty). Furthermore, the linear regression between ^{238}U and salinity using this sample set alone was statistically identical to that reported by Owens et al. [2011]. Finally, the measured average and standard deviation of the dissolved $^{234}U/^{238}U$ activity ratios was 1.1473 ± 0.0018, consistent within uncertainty with the global average (1.1468 ± 0.0001) [*Andersen et al.*, 2010]. This data can be accessed in the supplemental material.

4. Discussion

4.1 The Amazon plume

The outflow of the Amazon River has a dynamic impact on many chemical properties of the adjacent tropical Atlantic and Caribbean, such as salinity, silicate, nitrate and phosphate [*Froelich et al.*, 1978; *Edmond et al.*, 1981; *Demaster and Pope*, 1996]. While it was recognized

that the majority of river-borne Fe is removed from solution in estuarine mixing [*Boyle et al.*, 1977], recent field studies have confirmed elevated Fe concentrations in Amazon-influenced water (indicated by low salinities) up to 2000 km from the river mouth [*Rijkenberg et al.*, 2014; *Fitzsimmons et al.*, 2013; *Bergquist and Boyle*, 2006]. From GEOTRACES transect GA02, Rijkenberg et al. [2014] found a negative linear correlation among several stations intersecting the plume between salinity, S, and dissolved Fe, dFe (dFe [nmol/kg] = -0.11 x S [pss-78] + 4.99). This relationship is roughly consistent with the dFe and salinity observations reported by Fitzsimmons et al. [2013] and Bergquist and Boyle [2006]. Limited supply of Th from rivers through removal at estuaries has also been inferred from order of magnitude decreases in ^{232}Th concentrations from estuary to ocean in the Baltic Sea [*Andersson et al.*, 1995].

In the present transect, the three samples from stations 1 and 2 with low salinity anomalies near Barbados (at 10 or 25 m depth) had elevated dissolved ^{232}Th concentrations of 0.71, 0.96 and 1.00 pmol/kg. These concentrations are similar to those found in the water column near the Mauritanian margin in the eastern Atlantic [*Hayes et al.*, 2015a; *Anderson et al.*, 2016], which receives a much larger atmospheric dust input annually [*Ridley et al.*, 2012]. The Amazon outflow Th concentrations also scaled inversely with observed practical salinities of 34.71, 34.11 and 33.90, respectively. This high Th loading of the Amazon outflow water is consistent with some previous surface water measurements of particulate ^{232}Th of 0.27 and 0.46 pmol/kg [*Moran et al.*, 2002], considering particulate ^{232}Th is roughly 10-20% of dissolved ^{232}Th, as observed here. This riverine source of Th will clearly bias dust deposition estimates based on dissolved Th fluxes in this region. As mentioned, because the isotope composition (^{232}Th/^{230}Th) of riverine and atmospheric Th likely are not significantly different. Thus, these sources cannot be distinguished by Th data alone, although ^{228}Ra/^{226}Ra is known to be elevated in Amazon outflow

Formatted: Font: 12 pt

Formatted: Font: 12 pt

Formatted: Font: 12 pt

water [*Moore et al.*, 1986] and this could potentially be used as a correction factor, or at least a way to map out where dissolved Th fluxes will be based by coastal sources of Th.

The estimated dFe based on salinity for the three Amazon outflow samples for which we have dissolved Th data is 1.17, 1.24 and 1.26 nmol/kg, using the Rijkenberg et al [2014] correlation. This translates to dissolved Fe/Th mole ratios of 1658, 1293, 1257, respectively. The Fe/Th mole ratio of the upper continental crust is 15,500 ± 2,200, according to Rudnick and Gao [2014]. The Fe/Th ratio of Amazon River water is not well-characterized, but a near-crustal composition is a first assumption. Based on available measurements specific to Saharan dust (14,900 ± 2,100) [*Mahowald et al.*, 2005; *Muhs et al.*, 2007], this source is also consistent with an average crustal Fe/Th ratio. Thus from either source, dissolution of dust or leakage from the Amazon estuary, dissolved Fe is highly removed ~~in~~ from the waters influenced by the Amazon outflow near Barbados (roughly 10% of the source) using dissolved Th as indicator of Fe supply.

Using the calculated dissolved ^{232}Th fluxes in the mixed layer at stations 1 and 2, the Rudnick and Gao [2014] Fe/Th ratio, and equal fractional solubility, we estimate the dissolved Fe to this water was 250-300 µmol/m^2/yr. This flux is 5-10 times higher (and would be even higher if we used more deeply integrated dissolved ^{232}Th fluxes) than what state of the art models predict for the dissolved Fe flux from atmospheric deposition to this area (25-60 µmol/m^2/yr) [*Mahowald et al.*, 2009; *Myriokefalitakis et al.*, 2015]. Therefore despite the fact that the Amazon estuary is a major sink for riverine Fe, the Amazon outflow still provides a significant, perhaps dominant at times, supply of dissolved Fe to the adjacent ocean. With this incoming flux and the assumed Fe concentrations of 1.1-1.2 nmol/kg, this Fe has a residence time of 15-16 days, indicating extremely rapid uptake, likely driven by the high Fe demands of

Commented [EB7]: I suggest you quote Shokovitz, Price, and Boyle (1978) on Fe removal in the Amazon estuary. Sholkovitz E. R., Boyle E. A., and Price N. B. (1978) The removal of dissolved humic acids and iron during estuarine mixing. Earth and Planet. Sc. Lett. 40, 130-136.

Commented [EB8]: There are also papers on a strong Fe diagenetic cycle on the Amazon shelf (?Aller or some other Yale descendant)

the significant diazotroph population in this region [*Subramaniam et al.*, 2008; *Ward et al.*, 2013].

4.2 Colloidal content and Atlantic-Pacific comparison

In previous work, we hypothesized that one possible reason for the increasing dissolved ^{232}Th flux with integration depth could be the result of a predominance of colloidal Th in the upper water column, which might not obey the assumptions of the flux estimate method as colloidal Th could be quickly scavenged from the mixed layer and partially regenerated at depth [*Hayes et al.*, 2013, 2015b]. At the Hawaii Ocean Time-series station ALOHA, a relatively low dust deposition environment, this hypothesis was not supported, however, and we found a low proportion of dissolved Th was colloidal [*Hayes et al.*, 2015c].

In the relatively high dust deposition environment at station 6, a few degrees south of BATS, colloidal ^{232}Th contributed 1.5 ± 2.0 %, 6.4 ± 2.1 % and 5.4 ± 1.9 % to dissolved ^{232}Th at 10 m, 140 m (DCM) and 500 m depth, respectively (Fig. 6D). These are slightly smaller than the 10-20% proportions of colloidal ^{232}Th reported for the central North Pacific [*Hayes et al.*, 2015c], despite roughly an order of magnitude greater dust deposition and a factor of 6 greater dissolved ^{232}Th concentrations in the Atlantic (Fig. 6C). This is evidence that ^{232}Th released to seawater from dust is predominantly not in colloidal form, but is truly dissolved, or that any such colloids are smaller than 10 kDa (~20 nm). Colloidal ^{230}Th was also measured, pushing detection limits on the ~1 L samples, and is likely small (<3%), but was statistically indistinguishable from zero.

Interestingly, between station ALOHA and BATS, Fe does not have substantially different dissolved concentrations (Fig. 6A), despite the difference in dust deposition (and dissolved ^{232}Th concentrations). In the upper 50 m, dissolved Fe is in fact about 5 times higher at

Commented [EB9]: But keep in mind the seasonal variations in this discussion. As you know, surface Fe varies in Hawaii too.

BATS than at ALOHA (consistent with the factor ~6 difference in dissolved ^{232}Th). Below 100 m, however, the dissolved Fe profile down to 1000 m is nearly identical between the two sites, and thus the upper water column inventory is quite similar. If the dust-Fe is delivered in the mixed layer, it is likely very quickly buffered by biological uptake, ligand complexation and scavenging. Below the euphotic zone, Fe concentrations increase due to regeneration. Furthermore, at both BATS and ALOHA, colloidal Fe is greater than ~50% of the total dissolved all throughout the water column (Fig. 6B). If Fe is initially released from dust in the dissolved phase like Th, it is very quickly complexed by colloidal size ligands. In fact, its solubility in seawater may be limited by the availability of ligands, whereas this does not appear to be the case for Th. Future work is justified here, and perhaps could be progressed through kinetic response of Th and Fe to dust addition experiments.

4.3 Th solubility

As with Fe, the Th at stations 1 and 2 comes from a mixture of riverine and atmospheric sources whose proportions cannot be ascertained *a priori*. Therefore, we focus on the more northerly and more remote stations (Sts. 6 and 8) in order to use dissolved ^{232}Th fluxes to discern Th solubility. We could convert our aerosol Th measurements into deposition rates, using the traditionally technique of assuming an aerosol deposition rate, such as 1 cm/s or 1000 m/day. Then comparison of aerosol Th deposition with the local integrated dissolved Th flux would afford an in-situ estimate of fractional Th solubility. We did not encounter the Saharan dust plume, however, with the samples we collected over stations 6 and 8 on this cruise. Saharan dust deposition occurs in this area generally only in late Summer (July-September) [*Jickells et al.*, 1994]. Additionally, because the dissolved Th fluxes in the water column represent an average over the residence time of dissolved Th (3-5 years for 500 m depth, Fig. 4E), ideally an aerosol

384 deposition-dissolved flux comparison would be done with at least a seasonally-resolved, annual
385 average aerosol deposition.

386 Kadko et al. [2015] report seasonally resolved total (wet + dry) deposition of Fe at
387 Bermuda of 837 μmol/m^2/yr for the years 2011-2013 using the traditional assumed-deposition
388 rate method and 1680 μmol/m^2/yr using a new method based on atmospheric ^{7}Be flux. Assuming
389 this Fe is only from Saharan dust [*Arimoto et al.*, 2003], the expected aerosol Th deposition is
390 13-26 μg/m^2/yr. From the dissolved ^{232}Th fluxes at BATS (station 8), this comparison implies a
391 fractional Th solubility of 1.9-3.8% considering only the mixed layer, increasing to 14-28%
392 using fluxes integrated to the DCM (100 m) and 31-63% if using the integrated flux in the upper
393 500 m. While this range reflects both the uncertainties involved in estimating dissolved Th
394 fluxes (i.e., proper integration depth) and the uncertainties in converting aerosol loads into
395 depositions, clearly, a fractional Th solubility of 63% would be highly unexpected given the
396 insoluble nature of this element. With our best estimate being that integrating to the depth of the
397 DCM at least partially accounts for the Th export effect, we find it highly likely, however, that
398 the true effective Th solubility here is closer to the 14-28% range than the 1.9-3.8% range.

399 **5. Conclusion**

400 The dissolved Th isotopes offer a wealth of information about the flow of lithogenic
401 material to the ocean. In this study, we investigated how integrated fluxes of ^{232}Th based on
402 ^{230}Th scavenging rates, can be used to show the impact of the Amazon outflow and aerosol
403 deposition on surface ocean trace metal distributions. We found that only a small percentage of
404 dissolved Th exists in the colloidal size range even under conditions of high dust deposition
405 where dissolved Fe is substantially colloidal. Lastly, we found that frational Th solubility of

mineral dust is largely unconstrained, though likely in the range of 20%, and presents the greatest need for future research in dissolved metal proxies for mineral dust deposition.

Acknowledgements

This study was funded by the W. O. Crosby Postdoctoral fellowship (MIT) and The University of Southern Mississippi. The cruise was supported by UNOLS and an NSF grant to Maureen Conte. We also thank Karen Wishner, and all the Chief Science Training participants, especially co-chief scientists Jonathan Cohen and Paul Suprenand, for the combined efforts for planning and executing the cruise. Violetta Paba and Sam Monk operated the CTD/Niskin rosette and made available processed CTD data.

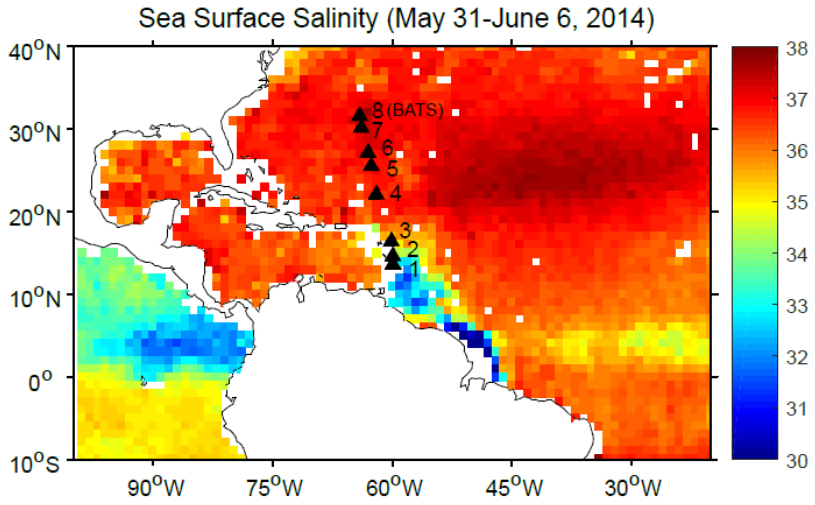

Figure 1. Map of stations sampled on the 2014 Chief Scientist Training workshop cruise between Barbados and Bermuda (AE1410). Water was collected at numbered stations and aerosols were collected during transits. Overlain is sea surface salinity (in practical salinity unitys) from Aquarius (Version 4, level-3 data gridded at 1 degree resolution), using the 7 day average for the period encompassing the 9-day cruise (May 31-June 8, 2014).

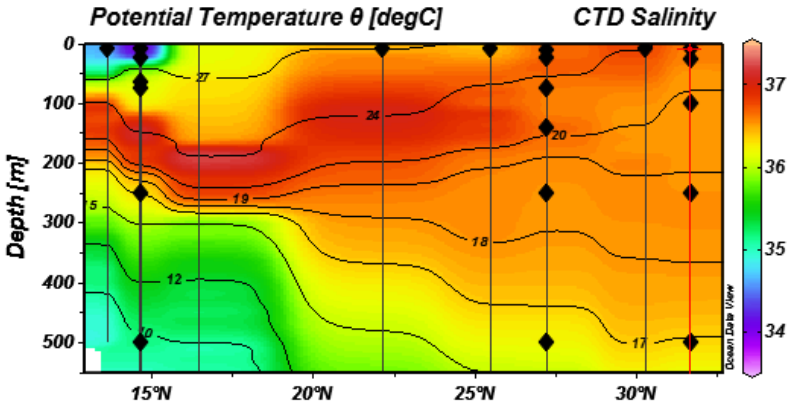

Figure 2. Practical salinity (colormap) and potential temperature (black contours) section along the transect indicated in Figure 1. The vertical lines represent CTD stations and the black diamonds are locations of water samples.

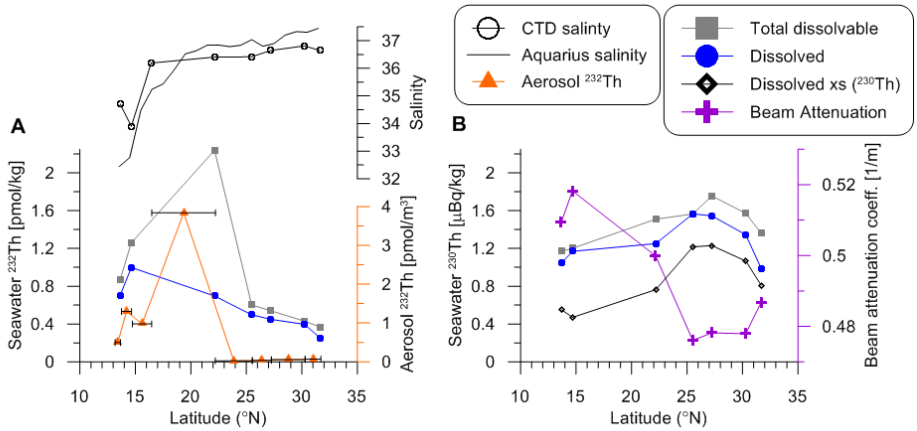

Figure 3. Surface transects of Th isotope data from AE1410. (A) Dissolved (filtered at 0.45 µm) and total dissolvable (unfiltered) ^{232}Th are distinguished by color and symbol in the legend. Seawater data is from 10 m water depth. The horizontal error bars for the aerosol ^{232}Th concentrations refer to the latitude range over which air was sampled during transits. The upper sub-plot shows that CTD salinity for each discrete sample in open circles and the solid line is the remotely-sensed salinity from the nearest grid cells of the weekly-averaged Aquarius data shown in Fig. 1. (B) Dissolved and total dissolvable ^{230}Th are distinguished as for ^{232}Th. Also shown, in black diamonds, is the dissolved excess ^{230}Th, which is defined using a correction for lithogenic material based on measured ^{232}Th. Dissolved ^{230}Th xs correlates well ($R^2 = 0.91$) with the beam

attenuation coefficient, a proxy for particle concentration. Vertical error bars for Th concentrations are roughly the size of symbol size and are omitted.

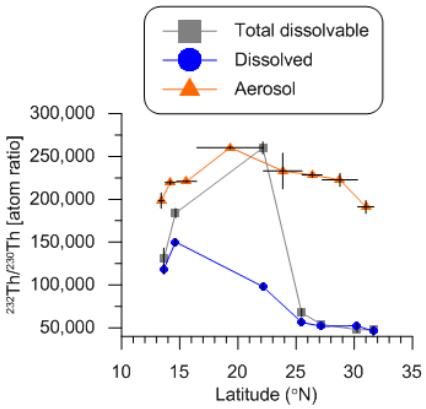

Figure 4. Surface transect (seawater data at 10 m water depth) from AE1410 of Th isotope ratios in seawater and aerosols.

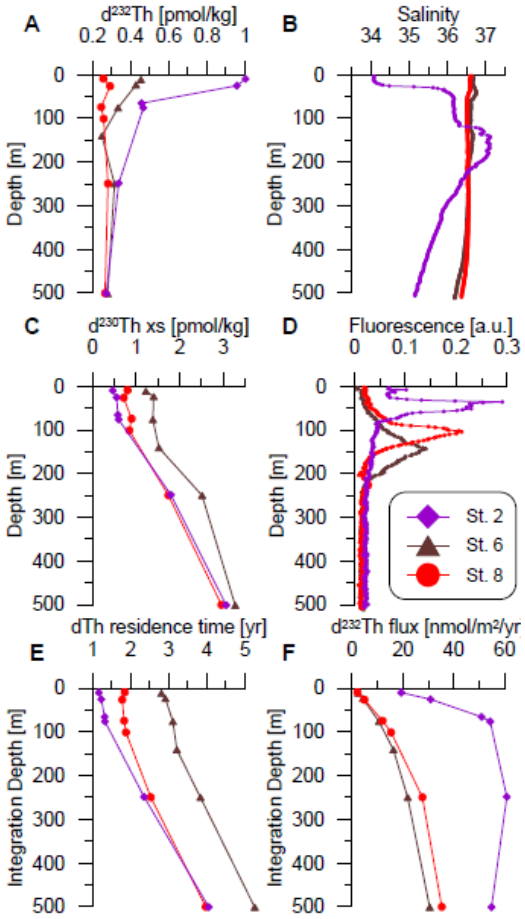

Figure 5. Depth profiles from AE410. (A) Dissolved ^{232}Th, (B) practical salinity binned at 1-m from CTD/Niskin cast, (C) dissolved ^{230}Th xs (corrected for lithogenic inputs), (D) fluorescence from CTD/Niskin cast in arbitrary units (a.u.), (E) dissolved Th residence time with respect to scavenging as a function of integration depth (F) dissolved ^{232}Th flux as a function of integration depth.

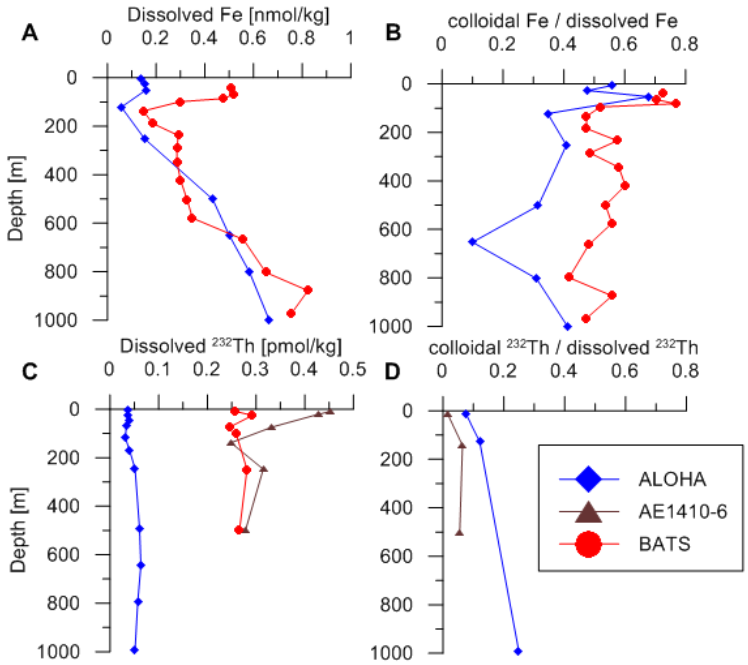

Figure 6. Thorium and iron depth profiles from the Bermuda and Hawaii Time-series stations, as well as nearby St. 6 (AE1410-6) of the present transect. (A) Dissolved Fe data from ALOHA [*Fitzsimmons et al.*, 2015a] and BATS [*Hatta et al.*, 2015]. (B) The fraction of dissolved Fe in the colloidal size fraction from ALOHA [*Fitzsimmons et al.*, 2015a] and BATS [*Fitzsimmons et al.*, 2015b]. (C) Dissolved ^{232}Th and colloidal fraction of dissolved (D) data from ALOHA [*Hayes et al.*, 2015c], BATS and AE1410-6 (this study).

Commented [EB10]: Of course, Fe at BATS cane show a large seasonal signal, and Hatta's data are from November while yours are from the summer.

Commented [EB11]: I suggest that you colorize the axis labels in red and blue to make it more obvious what is what.

References

Andersen, M. B., C. H. Stirling, and B. Zimmermann (2010), Precise determination of the open ocean ^{234}U/^{238}U composition, *Geochemistry Geophys. Geosystems*, *11*(12), Q12003, doi:10.1029/2010GC003318.

Anderson, R. F., M. Q. Fleisher, L. F. Robinson, R. L. Edwards, J. A. H. Q, and S. Bradley (2012), OCEANOGRAPHY : METHODS GEOTRACES intercalibration of for 10 Be Pa , and prospects, , doi:10.4319/lom.2012.10.XXX.

Anderson, R. F. et al. (2016), How well can we quantify dust deposition to the ocean?, *Philos. Trans. R. Soc. A Math. Phys. Eng. Sci.*, ???, ???

Andersson, P. S., G. J. Wasserburg, J. H. Chen, D. A. Papanastassiu, and J. Ingri (1995), ^{238}U-^{234}U and ^{232}Th-^{230}Th in the Baltic Sea and in river water, *Earth Planet. Sci. Lett.*, *130*, 217–234.

Arimoto, R., R. A. Duce, B. J. Ray, and U. Tomza (2003), Dry deposition of trace elements to the western North Atlantic, *Global Biogeochem. Cycles*, *17*(1), 1–10, doi:10.1029/2001GB001406.

Bergquist, B. A., and E. A. Boyle (2006), Iron isotopes in the Amazon River system: Weathering and transport signatures, *Earth Planet. Sci. Lett.*, *248*, 54–68, doi:10.1016/j.epsl.2006.05.004.

Bishop, J. K. (1986), The correction and suspended particulate matter calibration of Sea Tech transmissometer data, *Deep Sea Res.*, *33*, 121–134.

Blanke, B., M. Arhan, A. Lazar, and G. Prevost (2002), A Lagrangian numerical investigation of the origins and fates of the salinity maximum water in the Atlantic, *J. Geophys. Res.*, *107*(C10), 3163, doi:10.1029/2002JC001318.

Boyle, E. A., J. M. Edmond, and E. R. Sholkovitz (1977), The mechanism of iron removal in estuaries, *Geochim. Cosmochim. Acta*, *41*, 1313–1324.

Dammshäuser, A., T. Wagener, and P. L. Croot (2011), Surface water dissolved aluminum and titanium : Tracers for specific time scales of dust deposition to the Atlantic ?, *Geophys. Res. Lett.*, *38*, L24601, doi:10.1029/2011GL049847.

Demaster, D. J., and R. H. Pope (1996), Nutrient dynamics in Amazon shelf waters : results from AMASSEDS, *Cont. Shelf Res.*, *16*(3), 263–289.

Deng, F., A. L. Thomas, M. J. A. Rijkenberg, G. M. Henderson, R. Nioz, and A. B. Den Burg (2014), Controls on seawater ^{231}Pa , ^{230}Th and ^{232}Th concentrations along the flow paths of deep waters in the Southwest Atlantic, *Earth Planet. Sci. Lett.*, *390*, 93–102, doi:10.1016/j.epsl.2013.12.038.

Eden, C., and J. Willebrand (2001), Mechanism of interannual to decadal variability of the North Atlantic Circulation, *J. Clim.*, *14*, 2266–2279.

Edmond, J. M., E. A. Boyle, B. Grant, and R. F. Stallard (1981), The chemical mass balance in the Amazon plume I : The nutrients, *Deep Sea Res.*, *28A*(11), 1339–1374.

Fitzsimmons, J. N., R. Zhang, and E. A. Boyle (2013), Dissolved iron in the tropical North Atlantic Ocean, *Mar. Chem.*, *154*, 87–99, doi:10.1016/j.marchem.2013.05.009.

Fitzsimmons, J. N., C. T. Hayes, S. N. Al-subiai, R. Zhang, P. L. Morton, R. E. Weisend, and E. A. Boyle (2015a), Daily to decadal variability of size-fractionated iron and iron-binding ligands at the Hawaii Ocean Time-series Station ALOHA, *Geochim. Cosmochim. Acta*, *171*, 303–324, doi:10.1016/j.gca.2015.08.012.

Fitzsimmons, J. N., G. G. Carrasco, J. Wu, S. Roshan, M. Hatta, C. I. Measures, T. M. Conway, S. G. John, and E. A. Boyle (2015b), Partitioning of dissolved iron and iron isotopes into soluble and colloidal phases along the GA03 GEOTRACES North Atlantic Transect, *Deep. Res. Part II*, *116*, 130–151, doi:10.1016/j.dsr2.2014.11.014.

Froelich, P. N., D. K. Atwood, and G. S. Giese (1978), Influence of Amazon River discharge on surface salinity and dissolved silicate concentration in the Caribbean Sea, *Deep Sea Res.*, *25*, 735–744.

505 Gardner, W. D., P. E. Biscaye, J. P. V Zaneveld, and M. J. O. Richardson (1985), Calibration
506 and comparison of the LDGO nephelometer and the OSU transmissometer on the Nova
507 Scotian Rise, *Mar. Geol.*, *66*, 323–344.

508 Hatta, M., C. I. Measures, J. Wu, S. Roshan, J. N. Fitzsimmons, P. Sedwick, and P. Morton
509 (2015), An overview of dissolved Fe and Mn distributions during the 2010 – 2011 U . S .
510 GEOTRACES north Atlantic cruises : GEOTRACES GA03, *Deep. Res. Part II*, *116*, 117–
511 129, doi:10.1016/j.dsr2.2014.07.005.

512 Hayes, C. T., R. F. Anderson, M. Q. Fleisher, S. Serno, G. Winckler, and R. Gersonde (2013),
513 Quantifying lithogenic inputs to the North Pacific Ocean using the long-lived thorium
514 isotopes, *Earth Planet. Sci. Lett.*, *383*, 16–25, doi:10.1016/j.epsl.2013.09.025.

515 Hayes, C. T., R. F. Anderson, M. Q. Fleisher, K. F. Huang, L. F. Robinson, Y. Lu, H. Cheng, R.
516 L. Edwards, and S. B. Moran (2015a), ^{230}Th and ^{231}Pa on GEOTRACES GA03, the U.S.
517 GEOTRACES North Atlantic transect, and implications for modern and paleoceanographic
518 chemical fluxes, *Deep. Res. Part II Top. Stud. Oceanogr.*, *116*, 29–41.

519 Hayes, C. T. et al. (2015b), Intensity of Th and Pa scavenging partitioned by particle chemistry
520 in the North Atlantic Ocean, *Mar. Chem.*, *170*, 49–60.

521 Hayes, C. T., J. N. Fitzsimmons, E. A. Boyle, D. McGee, R. F. Anderson, R. Weisend, and P. L.
522 Morton (2015c), Thorium isotopes tracing the iron cycle at the Hawaii Ocean Time-series
523 Station ALOHA, *Geochim. Cosmochim. Acta*, *169*, 1–16.

524 Hellweger, F. L., and A. L. Gordon (2002), Tracing Amazon River water into the Caribbean Sea,
525 *J. Mar. Res.*, *60*(4), 537–549.

526 Hirose, K., and Y. Sugimura (1987), Thorium Isotopes in the Surface Air of the Western North
527 Pacific Ocean, *J. Environ. Radioact.*, *5*, 459–475.

528 Hsieh, Y., G. M. Henderson, and A. L. Thomas (2011), Combining seawater surface ocean Th
529 concentrations to determine dust fl uxes to the, *Earth Planet. Sci. Lett.*, *312*(3-4), 280–290,
530 doi:10.1016/j.epsl.2011.10.022.

531 Huh, C., J. M. Kelley, J. W. Murray, and C.-L. Wei (1994), Water column distribution of 230Th
532 and 232Th in the Black Sea, *Deep Sea Res. I*, *41*(1), 101–112.

533 Jickells, T., T. Church, A. Veron, and R. Arimoto (1994), Atmospheric inputs of manganese and
534 aluminium to the Sargasso Sea and their relation to surface water concentrations, *Mar.*
535 *Chem.*, *46*, 283–292.

536 Kadko, D., W. M. Landing, and R. U. Shelley (2015), A novel trace technique to quantify the
537 atmospheric flux of trace elements to remote ocean regions, *J. Geophys. Res. Ocean.*, *120*,
538 848–858, doi:10.1002/2014JC010314.

539 Lomas, M. W., N. R. Bates, R. J. Johnson, A. H. Knap, D. K. Steinberg, and C. A. Carlson
540 (2013), Two decades and counting: 24-years of sustained open ocean biogeochemical
541 measurements in the Sargasso Sea, *Deep. Res. Part II*, *93*, 16–32,
542 doi:10.1016/j.dsr2.2013.01.008.

543 Mahowald, N. M., A. R. Baker, G. Bergametti, N. Brooks, R. A. Duce, T. D. Jickells, J. M.

544 Prospero, and I. Tegen (2005), Atmospheric global dust cycle and iron inputs to the ocean,
545 *Global Biogeochem. Cycles*, *19*, GB4025, doi:10.1029/2004GB002402.

546 Mahowald, N. M. et al. (2009), Atmospheric Iron Deposition: Global Distribution, Variability,
547 and Human Perturbations, *Ann. Rev. Mar. Sci.*, *1*, 245–278,
548 doi:10.1146/annurev.marine.010908.163727.

549 Maiti, K., C. R. B. Nelson, and K. O. Buesseler (2010), Insights into particle formation and
550 remineralization using the short-lived radionuclide , Thoruim-234, *Geophys. Res. Lett.*, *37*,
551 L15608, doi:10.1029/2010GL044063.

552 Measures, C. I., and E. T. Brown (1996), Estimating dust input to the Atlantic Ocean using
553 surface water aluminum concentrations, in *The Impact of Desert dust Across the*
554 *Mediterranean*, edited by S. Guerzoni and R. Chester, pp. 301–311, Kluwer Academic
555 Publishers.

556 Measures, C. I., and S. Vink (2000), On the use of dissolved aluminum in surface waters to
557 estimate dust deposition to the ocean, *Global Biogeochem. Cycles*, *14*(1), 317–327.

558 Moore, S., J. L. Sarmiento, and R. M. Key (1986), Tracing the Amazon component of surface
559 Atlantic water using ^{228}Ra, salinity and silica, *J. Geophys. Res.*, *91*, 2574–2580.

560 Moran, S. B., C. Shen, H. N. Edmonds, S. E. Weinstein, J. N. Smith, and R. L. Edwards (2002),
561 Dissolved and particulate ^{231}Pa and ^{230}Th in the Atlantic Ocean : constraints on intermediate
562 / deep water age, boundary scavenging, and ^{231}Pa / ^{230}Th fractionation, *Earth Planet. Sci.*
563 *Lett.*, *203*, 999–1014.

564 Morton, P. L., W. M. Landing, S. Hsu, A. Milne, A. M. Aguilar-islas, A. R. Baker, and A. R.
565 Bowie (2013), Methods for the sampling and analysis of marine aerosols: results from the
566 2008 GEOTRACES aerosol intercalibration experiment, *Limnol. Oceanogr. Methods*, *11*,
567 62–78, doi:10.4319/lom.2013.11.62.

568 Muhs, D. R., J. R. Budahn, J. M. Prospero, and S. N. Carey (2007), Geochemical evidence for
569 African dust inputs to soils of western Atlantic islands : Barbados , the Bahamas, and
570 Florida, *J. Geophys. Res.*, *112*, F02009, doi:10.1029/2005JF000445.

571 Myriokefalitakis, S., N. Daskalakis, N. Mihalopoulos, A. R. Baker, A. Nenes, and M. Kanakidou
572 (2015), Changes in dissolved iron deposition to the oceans driven by human activity : a 3-D
573 global modelling study, *Biogeosciences*, *12*, 3973–3992, doi:10.5194/bg-12-3973-2015.

574 Owens, S. A., K. O. Buesseler, and K. W. W. Sims (2011), Re-evaluating the 238 U-salinity
575 relationship in seawater : Implications for the U – 234 Th disequilibrium method, *Mar.*
576 *Chem.*, *127*(1-4), 31–39, doi:10.1016/j.marchem.2011.07.005.

577 Pham, M. K., J. J. La Rosa, S.-H. Lee, B. Oregioni, and P. P. Povinec (2005), Deposition of
578 Saharan Dust in Monaco Rain 2001–2002: Radionuclides and Elemental Composition,
579 *Phys. Scr.*, (T118), 14–17.

580 Poole, R., and M. Tomczak (1999), Optimum multiparameter analysis of the water mass
581 structure in the Atlantic Ocean thermocline, *Deep. Res. Part I*, *46*, 1895–1921.

582 Reuer, M. K., E. A. Boyle, and B. C. Grant (2003), Lead isotope analysis of marine carbonates

583 and seawater by multiple collector ICP-MS, *Chem. Geol.*, *200*, 137–153,
584 doi:10.1016/S0009-2541(03)00186-4.

585 Ridley, D. A., C. L. Heald, and B. Ford (2012), North African dust export and deposition : A
586 satellite and model perspective, *J. Geophys. Res.*, *117*, D02202,
587 doi:10.1029/2011JD016794.

588 Rijkenberg, M. J. A., R. Middag, P. Laan, L. J. A. Gerringa, H. M. Van Aken, J. T. M. De Jong,
589 and H. J. W. De Baar (2014), The Distribution of Dissolved Iron in the West Atlantic
590 Ocean, *PLoS One*, *9*(6), 1–14, doi:10.1371/journal.pone.0101323.

591 Roy-Barman, M., J. H. Chen, and G. J. Wasserburg (1996), ^{230}Th-^{232}Th systematics in the central
592 Pacific Ocean: The sources and fates of thorium, *Earth Planet. Sci. Lett.*, *139*, 351–363.

593 Roy-Barman, M., C. Lemaître, S. Ayrault, C. Jeandel, M. Souhaut, and J. Miquel (2009), The
594 influence of particle composition on Thorium scavenging in the Mediterranean Sea, *Earth*
595 *Planet. Sci. Lett.*, *286*(3-4), 526–534, doi:10.1016/j.epsl.2009.07.018.

596 Rudnick, R. L., and S. Gao (2014), *Composition of the Continental Crust*, 2nd ed., Elsevier Ltd.

597 Shiller, A. M., and G. R. Bairamadgi (2006), Dissolved gallium in the northwest Pacific and the
598 south central Atlantic Ocean: Implications for aeolian Fe input and a reconsideration of
599 profiles, *Geochemistry Geophys. Geosystems*, *7*, Q08M09, doi:10.1029/2005GC001118.

600 Steven, D. M., and A. L. Brooks (1972), Identification of Amazon River water at Barbados, W.
601 Indies, by salinity and silicate measurements, *Mar. Biol.*, *348*, 345–348.

602 Subramaniam, A. et al. (2008), Amazon River enhances diazotrophy and carbon sequestration in
603 the tropical North Atlantic Ocean, *Proc. Natl. Acad. Sci. U.S.A.*, *105*(30), 10460–10465,
604 doi:10.1029/2006GB002751.

605 Swarzenski, P., P. Campbell, D. Porcelli, and B. McKee (2004), The estuarine chemistry and
606 isotope systematics of ^{234,238}U in the Amazon and Fly Rivers, *Cont. Shelf Res.*, *24*, 2357–
607 2372, doi:10.1016/j.csr.2004.07.025.

608 Ward, B. A., S. Dutkiewicz, C. M. Moore, and M. J. Follows (2013), Iron, phosphorus, and
609 nitrogen supply ratios define the biogeography of nitrogen fixation, *Limnol. Oceanogr.*,
610 *58*(6), 2059–2075, doi:10.4319/lo.2013.58.6.2059.

611